ARTICLE IN PRESS
RSE-09415; No of Pages 14
Remote Sensing of Environment xxx (2015) xxx–xxx
Contents lists available at ScienceDirect
Remote Sensing of Environment
journal homepage: www.elsevier.com/locate/rse

A multi-temporal spectral library approach for mapping vegetation species across spatial and temporal phenological gradients

Kenneth L. Dudley [a,*], Philip E. Dennison [a], Keely L. Roth [b], Dar A. Roberts [c], Austin R. Coates [a]

[a] Department of Geography, University of Utah, United States
[b] Department of Land, Air and Water Resources, University of California Davis, United States
[c] Department of Geography, University of California Santa Barbara, United States

ARTICLE INFO

Article history:
Received 26 June 2014
Received in revised form 10 May 2015
Accepted 14 May 2015
Available online xxxx

Keywords:
HyspIRI
Species classification
Endmember selection
MESMA
Hyperspectral time series
Vegetation phenology
AVIRIS
Mediterranean ecosystems

ABSTRACT

Variability in spectral reflectance due to spatial and temporal gradients in vegetation phenology presents issues for accurate vegetation classification. Phenological variability through space and over time can result in misclassification when spectra from non-representative areas or times are used as training data. Vegetation classification at the species level could benefit from introducing phenological information to spectral libraries, but utilization of this information across multiple dates of imagery will require new approaches to building spectral libraries and to classification. This paper explores an automated method for selecting a single multi-temporal spectral library that can be used to classify vegetation species across multiple dates within an image time series. Iterative Endmember Selection (IES) was used to select spectra from Airborne Visible Infrared Imaging Spectrometer (AVIRIS) data acquired on five dates in the same year. IES selected spectra to maximize species classification accuracy (as measured by Kappa) within a multi-temporal spectral library that included spectra from all image dates. The resulting multi-temporal endmember library was applied using Multiple Endmember Spectral Mixture Analysis (MESMA) to classify vegetation species and land cover across all five images. Results indicate that multi-temporal, seasonally-mixed spectral libraries achieved similar overall classification accuracy compared to single-date libraries, and in some cases, resulted in improved classification accuracy. Several species had increased Producer's or User's accuracy using a multi-temporal library, while others had reduced accuracy compared to same-date classifications. The image dates of endmembers used to map species in each image were examined to determine if this information could improve our understanding of phenological spectral differences for specific species. Multi-temporal endmember libraries could provide a means for mapping species in data where phenology, climatic variability, or spatial gradients are not known in advance or may not be easily accounted for by endmembers from a single date. New missions, such as the proposed Hysperspectral Infrared Imager (HyspIRI) mission, will provide greatly improved access to multi-temporal spectral datasets and new opportunities for mapping vegetation spectral variability on regional-to-global scales.

1. Introduction

One of the challenges of classifying vegetation using remote sensing techniques is the changing spectral response of vegetation due to phenology; defined herein as the seasonal change in biological life as a result of changing environmental conditions (Lieth, 1974). Spectral feature based classification and mapping techniques readily applied to features that tend not to change greatly over time (e.g. geologic features, urban materials) are more difficult to apply to vegetation because of seasonal and climate-induced changes that result in variability in spectral reflectance over space and time (Dennison & Roberts, 2003a). For example, timing of green-up and senescence may vary along elevation and/or precipitation gradients.

Vegetation phenology contains useful information about broad plant species composition and vegetation health. Species composition, phenoregion modeling, and plant functional type classification can be carried out using multi-temporal vegetation indices from multispectral sensors such as the Landsat series (Mannel & Price, 2012; Walker, de Beurs, & Wynne, 2014; Zhong, Gong, & Biging, 2012) and the Moderate Resolution Imaging Spectroradiometer (MODIS) (Potgieter, Apan, Dunn, & Hammer, 2007; Wardlow & Egbert, 2010; Zhang, Zhang, & Xu, 2012). Hyperspectral imagery provides more detailed spectral information, and has been successfully used to map vegetation at the species level (Cochrane, 2000; Dehaan, Louis, Wilson, Hall, & Rumbachs, 2007; Ishii et al., 2009; López-Granados, Jurado-Expósito, Peña-Barragan, & García-Torres, 2006; Ullah, Schlerf, Skidmore, & Hecker, 2012; Yamano, Chen, & Tamura, 2003). Applications of hyperspectral data for species mapping include tree taxa in the Amazon Basin (Papeş, Tupayachi, Martínez, Peterson, & Powell, 2010), invasive species in the California

* Corresponding author.

http://dx.doi.org/10.1016/j.rse.2015.05.004
0034-4257/

Please cite this article as: Dudley, K.L., et al., A multi-temporal spectral library approach for mapping vegetation species across spatial and temporal phenological gradients, *Remote Sensing of Environment* (2015), http://dx.doi.org/10.1016/j.rse.2015.05.004

Delta ecosystem (Hestir et al., 2008), tropical tree species in Costa Rica (Clark, Roberts, & Clark, 2005) and several species in southern California chaparral (Dennison & Roberts, 2003a; Roberts, Dennison, Roth, Dudley, & Hulley, 2015; Roberts et al., 1998). Hyperspectral datasets have also been used to determine spectral separability between vegetation types in Hawaiian forests (Asner, Jones, Martin, Knapp, & Hughes, 2008) and coastal wetlands (Schmidt & Skidmore, 2003; Zomer, Trabucco, & Ustin, 2009).

Relatively little research has been conducted on the capability of multi-temporal hyperspectral imagery to identify vegetation at the species level, primarily due to a lack of repeated sampling of large areas (Dennison & Roberts, 2003a). Species phenology, its impact on spectral reflectance, and its spatial and temporal variability are important considerations for classifying species. Hestir et al. (2008) found that the life history of vegetation species under study was an important component in classification, and that identification based on known flowering, fruiting, and senescing timing of certain species improved classification accuracy. A study by Mannel and Price (2012) compared land cover classification accuracy between summer AVIRIS and two season (spring/fall) Landsat TM imagery using decision tree classification for the Black Hills, South Dakota. Their study found that while summer AVIRIS data provided the best single date accuracy (85%), accuracies for the combined multi-temporal Landsat TM dataset were higher (89%), despite its lack of spectral resolution. Mannel and Price (2012) concluded that seasonality may be a more important factor for identifying land cover types than hyperspectral data alone.

The proposed Hyperspectral Infrared Imager (HyspIRI) mission, with global coverage of Earth's land surfaces and a 19-day repeat acquisition cycle, will provide new opportunities for mapping vegetation species on a seasonal basis. Spatial and temporal variability in vegetation reflectance occurs across spatial scales ranging from local (e.g. mountain slopes) to global (e.g. latitudinal precipitation gradients). One potential method for dealing with spatial and temporal variability in vegetation reflectance due to phenology is to combine classification training data from multiple image dates while minimizing confusion between classes across all dates. Using a multi-temporal spectral library approach applied to hyperspectral data, it may be possible to map vegetation at the species level regardless of the seasonality of the input image. The objective of this study was to evaluate the ability of a multi-temporal endmember library that accounts for variability in vegetation reflectance to accurately map vegetation species and land cover across multiple image dates. We found that a single, multi-temporal endmember library selected from five Airborne Visible Infrared Imaging Spectrometer (AVIRIS) images collected over the same area during a single year was able to classify species with only minor changes in map accuracy.

2. Methods

2.1. Study area

The study area encompassed the Santa Barbara, California, USA coast, the Santa Ynez Mountain Range, and inland areas extending across the Santa Ynez Valley to Zaca Peak in Los Padres National Forest (Fig. 1). The study area spanned an elevation gradient from sea level to a peak of 1311 m. Climate for this region is Mediterranean type with dry, warm summers and moist, cool winters. Rainfall in Santa Barbara averages 472 mm, but is strongly dependent on elevation, with higher rainfall in the Santa Ynez Mountains and decreased rainfall in the lee of this range. This topographically diverse region supports a mosaic of oak woodland, grassland, and shrubland consisting of evergreen chaparral (*Adenostoma fasciculatum*, *Arctostaphylos glauca*/*glandulosa*, *Ceanothus* spp., and *Quercus berberidifolia*) and coastal sage scrub (Franklin, Regan, & Syphard, 2014). Coastal sage scrub is characterized by significant vegetation diversity, dominated by drought-deciduous shrubs (*Artemisia californica* and *Salvia* spp.) mixed with succulent and evergreen species, and a herbaceous understory (Riordan & Rundel, 2014). *Quercus agrifolia* dominates in oak woodlands while *Platanus racemosa*, *Umbellularia californica*, and *Salix* spp. comprise the majority of riparian zones and canyon drainages.

2.2. Image acquisition

Imagery used for this project was a time-series of AVIRIS data consisting of five separate dates in 2009: March 10, March 30, May 8, June 17, and August 26. These images represent the most comprehensive intra-annual hyperspectral time series data that were available at the time of this study and may not reflect ideal acquisition dates for any given phenology. Images were separated into three separate flight paths per date (Table 1). A North to South swath (f1) ranged from Zaca Peak to the coastline, an East to West swath (f2) covered the inland portion of the Santa Ynez Mountains, and a second East to West swath (f3) covered Santa Barbara and the remaining coastline (Fig. 1). There were a total of fifteen images acquired on five dates (Table 1). Images were processed to calibrated radiance and initial orthorectification was done by the NASA Jet Propulsion Laboratory. Orthorectification

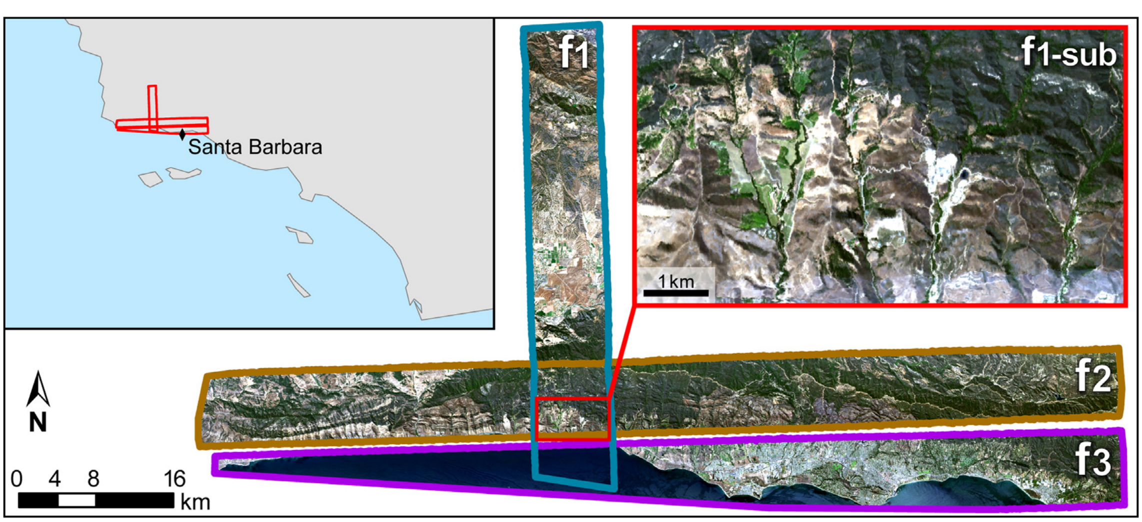

Fig. 1. Study region near Santa Barbara, California, USA (inset map, upper left) with true color composites of the AVIRIS imagery collected 26 Aug 2009. Individual flight paths reduced to overlapping spatial extents common to all dates are bordered and denoted by f1, f2, and f3. The subregion "f1-sub" outlined in red was taken from images in swath "f1" and is used for visualization in subsequent figures. (For interpretation of the references to color in this figure legend, the reader is referred to the web version of this article.)

Please cite this article as: Dudley, K.L., et al., A multi-temporal spectral library approach for mapping vegetation species across spatial and temporal phenological gradients, *Remote Sensing of Environment* (2015), http://dx.doi.org/10.1016/j.rse.2015.05.004

Table 1
Fifteen AVIRIS flightlines acquired in 2009 and used for the analysis. Swaths labeled "f1", "f2", and "f3" correspond to the swaths shown in Fig. 1.

Image date	Flightline	Swath	Pixel size (m)	Solar zenith (°)	Solar azimuth (°)
10 Mar	090310r07	f1	16.0	43.2	210.9
10 Mar	090310r08	f2	15.7	45.3	216.8
10 Mar	090310r09	f3	16.4	47.3	221.5
30 Mar	090330r07	f1	16.0	31.0	172.4
30 Mar	090330r09	f2	15.8	31.4	194.2
30 Mar	090330r08	f3	16.4	30.6	181.9
8 May	090508r11	f1	11.1	17.6	183.4
8 May	090508r10	f2	10.9	17.8	166.7
8 May	090508r12	f3	11.5	18.4	201.6
17 Jun	090617r07	f1	11.2	14.2	220.4
17 Jun	090617r06	f2	11.1	12.2	205.2
17 Jun	090617r08	f3	11.5	17.9	236.1
26 Aug	090826r08	f1	11.3	27.7	212.0
26 Aug	090826r09	f2	11.2	30.2	221.6
26 Aug	090826r10	f3	11.7	32.8	228.5

Table 2
Land cover/species classes, abbreviated name, number of polygons in each class (NP), and the total area in km^2 covered by the polygons for each class. Numbers of pixels for each class vary by date depending on pixel size (Table 1). Thirteen polygons sampled twice due to overlap between f1 and f2 are not included in totals.

Class	Abbrev.	NP	km^2
Adenostoma fasciculatum	ADFA	28	0.338
Artemisia californica–Salvia leucophylla	ARCA-SALE	14	0.275
Arctostaphylos glauca/glandulosa	ARGL	15	0.274
Baccharis pilularis	BAPI	13	0.055
Brassica nigra	BRNI	13	0.378
Ceanothus cuneatus	CECU	13	0.110
Ceanothus megacarpus	CEME	20	0.307
Ceanothus spinosus	CESP	13	0.163
Citrus spp.	CISP	15	0.110
Eriogonum fasciculatum	ERFA	13	0.277
Eucalyptus spp.	EUSP	15	0.270
Irrigated Grass (mixed species)	IRGR	14	0.136
Mediterranean annual grasses and forbs	MAGF	12	0.604
Persea americana	PEAM	18	0.152
Pinus sabiniana	PISA	15	0.205
Platanus racemosa	PLRA	14	0.299
Quercus agrifolia	QUAG	5	0.062
Quercus douglasii	QUDO	17	0.313
Rock	ROCK	12	0.062
Soil	SOIL	11	0.128
Umbellularia californica	UMCA	9	0.095
Total polygons/area		299	4.612

was improved using additional tie points. All flightlines were acquired during the same year such that the sensor response function did not change between dates. Apparent surface reflectance was retrieved using ATCOR4 (Richter & Schläpfer, 2002). ATCOR corrects for directional reflectance using a digital elevation model to account for sun-sensor geometry, including solar zenith angle which varied by date and swath (Table 1). Fifty bands with poor signal-to-noise ratio and strong water vapor absorptions were removed and the remaining 174 bands were used in the analysis.

Images were masked to limit analysis to overlapping spatial extents that had data on every date. A single spatial resolution was not used across all flightlines and dates, as there was no common spatial resolution that would result in a uniform spatial resampling. Weighted resampling would result in a much coarser spatial resolution, which would have eliminated several species from mapping due to limited training polygons. The original spatial resolution was maintained to ensure that spectra from each image were as pure at the canopy level as possible. Schaaf, Dennison, Fryer, Roth, and Roberts (2011) found that endmembers extracted from resampled images with differing spatial resolutions could affect classification accuracy, with endmembers extracted at coarser resolution performing poorly relative to endmembers extracted at finer resolution. The impact of the range of spatial resolutions in this study (10.9–16.7 m) on classification accuracy is unknown, although the range in spatial resolutions is much smaller than the 20–60 m range investigated by Schaaf et al. (2011).

2.3. Ground reference data

Reference data used for this project are described by Roth, Dennison, and Roberts (2012) and were collected during field campaigns in 2003, 2009, and 2012. Species dominance was estimated using methods adapted from Meentemeyer and Moody (2000), where vegetation patches having 75% or greater single-species composition were observed and recorded using a spotting scope. Orchards, irrigated grass, soil, rock, and Mediterranean annual grasses and forbs were digitized from 1 m orthoimagery. The reference data include 299 polygons with 21 unique classes (Table 2). Thirteen polygons were sampled twice where flight lines overlapped (f1 and f2) for classes MAGF, ADFA, CESP, CISP, ROCK, and PEAM, creating a total of 312 reference polygons.

2.4. Spectral library development

Polygon data and metadata were processed in VIPER Tools 1.5 (www.vipertools.org). VIPER Tools is an IDL-based ENVI (Exelis Visual Information Solutions) extension which is used to create and edit spectral libraries extracted from imagery, calculate endmember RMSE values modeling all other spectra in a spectral library (stored as a "square array", Dennison & Roberts, 2003b), and execute Multiple Endmember Spectral Mixture Analysis (MESMA) classification. VIPER Tools code was run-time optimized and modified to take advantage of multicore processors, permitting processing of libraries with many thousands of spectra. A single set of georeferenced polygons was used for all images and all image dates (Table 2); the polygons were checked for consistency between image dates to ensure that land cover had not changed between dates. Spectra were extracted from each image separately using the reference polygons, and then combined into five single-date reference libraries. The single-date reference libraries were individually tested for duplicate spectra caused by orthorectification and all duplicates were removed from each reference library. For the March and May images less than 0.2% of reference library spectra had corrupted spectra in the near infrared region due to a data collection artifact; these pixels were removed from the analysis.

The single-date reference libraries were divided into five training and five validation libraries using a random sampling algorithm proposed by Roth et al. (2012), which extracts a set percentage of randomly selected spectra from each polygon for use as a training library. The remaining non-training spectra comprise the validation library and are used to assess classification accuracy. Given different pixel sizes between image dates (Table 1), the number of useable spectra was considerably different for March images. Approximately 50% of reference spectra were randomly selected for training libraries from the March dates (Table 3). Extraction percentages were then adjusted downward for the remaining dates to maintain similarly sized training libraries across all dates (Table 3). The single-date training libraries were combined into a single, large multi-temporal training library consisting of 49,427 spectra.

2.5. Iterative Endmember Selection (IES) and Multiple Endmember Spectral Mixture Analysis (MESMA)

Spectral mixing occurs when the spatial resolution of a sensor is coarse enough that differing surface materials appear within the same pixel (Keshava & Mustard, 2002). At both coarse and fine spatial scales, spectral mixing of vegetation occurs when the spectral components, which comprise a pixel, are mixed from different sources, such as leaf, branch, and ground surface spectra. Spectral Mixture Analysis (SMA) is a method for analyzing and separating out the constituent

Table 3
Image acquisition dates, the total size of the reference library, and the number of spectra divided between training and validation libraries. The final number of spectra chosen by Iterative Endmember Selection (IES) for endmember libraries (IES EM) run with an RMSE threshold of 0.01, and the resulting Kappa values (IES Kappa) are also shown. The combined multi-temporal training library and IES endmember library are shown in the "MT" row.

Image date	Reference spectra	Training spectra	Validation spectra	IES EM	IES kappa
10 Mar	20,497	9868	10,629	1365	0.826
30 Mar	20,017	9928	10,089	1282	0.854
8 May	33,045	9878	23,167	1311	0.835
17 Jun	33,719	9874	23,845	1030	0.875
26 Aug	33,297	9879	23,418	1223	0.847
MT		49,427		5379	0.855

components of a pixel by determining the fraction of endmembers which contribute to the spectral signature in a given pixel (Keshava & Mustard, 2002). Endmembers are representative spectra used as proxies to identify materials on the ground (Tompkins, Mustard, Pieters, & Forsyth, 1997), and are sometimes referred to as "pure" spectra of the reference material used for SMA. Endmembers can be selected from imagery (Somers, Zortea, Plaza, & Asner, 2012; Youngentob et al., 2011), collected from field spectroscopy (Nidamanuri & Zbell, 2011; Okin, Clarke, & Lewis, 2013), extracted from laboratory measurements (Roberts, Smith, & Adams, 1993), or simulated with radiative transfer models (Dennison, Charoensiri, Roberts, Peterson, & Green, 2006; Sonnentag et al., 2007).

In linear SMA, spectra are modeled through the summation of endmembers, which are weighted by the fractional endmember components required to produce the spectral mixture observed (Adams, Smith, & Gillespie, 1993):

$$\rho'_\lambda = \sum_{i=1}^{N} f_i * \rho_{i\lambda} + \varepsilon_\lambda \quad (1)$$

where ρ'_λ is the reflectance of a pixel and is the sum of the reflectance of each endmember $\rho_{i\lambda}$ within a pixel, where N is the number of endmembers, multiplied by its fractional cover f_i. The unmodeled portions of the spectrum are expressed in the residual term, ε_λ. Root mean square error (RMSE) is calculated to determine the model fit:

$$\mathrm{RMSE} = \sqrt{\frac{\sum_{k=1}^{B} (\varepsilon_{i\lambda})^2}{B}} \quad (2)$$

where B is the number of bands and k is the band number. Linear SMA models assume that the light reflecting off materials within a pixel only interacts with a single material and that the resulting mixture can be modeled as a linear sum of each endmember weighted by its fractional cover (Borel & Gerstl, 1994; Keshava & Mustard, 2002; Ray & Murray, 1996; Roberts et al., 1993).

Multiple Endmember Spectral Mixture Analysis (MESMA) is a spectral mixing model which allows endmembers to vary in type and number on a per pixel basis (Dennison & Roberts, 2003b; Roberts et al., 1998). MESMA improves on SMA by unmixing images with the best fit (lowest RMSE) combinations of endmembers for each pixel. MESMA can also require that modeled pixels meet minimum spectral fit, fraction, and residual constraints (Roberts et al., 1998). MESMA-based spectral unmixing methods have been used to assess semi-arid shrub, heathlands, and scrub vegetation (Delalieux et al., 2012; Hamada, Stow, Roberts, Franklin, & Kyriakidis, 2012; Liao, Zhang, & Liu, 2012; Roberts et al., 1998; Thorp, French, & Rango, 2013), map urban and impervious areas (Franke, Roberts, Halligan, & Menz, 2009; Powell, Roberts, Dennison, & Hess, 2007; Roberts, Quattrochi, Hulley, Hook, & Green, 2012), research coastal marshes and wetlands (Li, Ustin, & Lay, 2005; Michishita, Gong, & Xu, 2012; Rosso, Ustin, & Hastings, 2005), and monitor invasive species (Somers & Asner, 2012, 2013). Using a two endmember model (one shade endmember and one non-shade endmember), MESMA can be used as a classification method that accounts for variations in brightness between endmembers and pixel spectra. This study uses two endmember MESMA to classify vegetation species and land cover classes.

Iterative Endmember Selection (IES) is an automated technique developed to facilitate quantitatively selected, representative endmembers for image classification using two endmember MESMA (Roth et al., 2012; Schaaf et al., 2011). For this research the IES algorithm was streamlined and improved to utilize parallel processing for faster runtime, though the basic process remains the same. IES uses an RMSE threshold to identify the endmembers that best model the spectra in a training library. Accuracy is then determined using Kappa (Cohen, 1960), a discrete multivariate statistical technique for assessing concordance in categorical data (Congalton, 1991). IES first selects a single endmember with the highest initial Kappa value from a training library. The remaining endmembers are then added and subtracted from the initial endmember to identify the set of endmembers which further increases Kappa values (Roth et al., 2012). The final result from IES is a representative endmember library which is optimized from the training library (Schaaf et al., 2011). Since IES selects only those endmembers which increase Kappa within a training library, within-class accuracy is not optimized and endmembers for certain classes may not be represented in the final endmember library if the addition of that class reduces the overall Kappa value. Methods for forcing the selection of classes in IES exist (Roth et al., 2012), but since the overall goal of IES is to maximize classification accuracy with MESMA (Schaaf et al., 2011), the tradeoff of not representing some classes may be acceptable.

IES was used to select a multi-temporal endmember library from the multi-temporal training library. For comparison, IES was also used to select single-date endmember libraries from each single-date training library. IES used a square array of RMSE values (Eq. (2)) showing each endmember in a library modeled against all other spectra in the library (Dennison & Roberts, 2003b). Endmembers with a lower RMSE in the square array are more similar, while endmembers with higher RMSE are more dissimilar. Endmembers which model the fewest spectra of a different class produce higher Kappa statistic values and tend to be selected for inclusion in an IES spectral library.

Past studies (Dennison & Roberts, 2003a,b; Roberts et al., 1998; Roth et al., 2012; Schaaf et al., 2011) have used an RMSE threshold of 0.025 to determine if an endmember correctly modeled other spectra in training libraries. If RMSE exceeds this threshold, the spectrum is labeled as unmodeled. Various RMSE thresholds were tested to determine the overall classification accuracy for the training libraries. At a 0.025 RMSE threshold the average overall classification accuracy ranged between 50 and 60%. An RMSE threshold of 0.01 provided a higher overall accuracy of 68 to 76%, and was used for this analysis. There was a tradeoff in selecting a more stringent RMSE threshold; the size of the output IES endmember library increased as RMSE threshold was decreased, since each selected endmember modeled fewer spectra in the training library. The sizes of the input reference libraries and final IES endmember libraries are shown in Table 3.

All image swaths were classified individually with MESMA via VIPER Tools using the IES derived multi-temporal and single-date endmember libraries. MESMA was run with fractional constraints for the minimum allowable endmember fraction (−0.05), maximum allowable endmember fraction (1.05), maximum allowable shade fraction (0.80), and RMSE (0.01). All constraint values except the RMSE constraint were based on values used in previous studies (Li et al., 2005; Roth et al., 2012; Schaaf et al., 2011; Thorp et al., 2013).

Please cite this article as: Dudley, K.L., et al., A multi-temporal spectral library approach for mapping vegetation species across spatial and temporal phenological gradients, *Remote Sensing of Environment* (2015), http://dx.doi.org/10.1016/j.rse.2015.05.004

2.6. Accuracy assessment and endmember temporal analysis

Results of the classifications were tested using the independent validation libraries unique to each date. A confusion matrix was calculated and used to determine User's accuracy and Producer's accuracy. User's accuracy shows errors of commission and Producer's accuracy shows errors of omission (Janssen & van der Wel, 1994). Errors of omission are reference pixels which should have been classified a particular class but were not assigned that class, while errors of commission occur when classified pixels are classified wrongly (Janssen & van der Wel, 1994).

For images classified using the multi-temporal endmember library, the date of the endmember used to model each validation pixel was examined. Correctly classified pixels, based on the validation data, were extracted from the dataset and plotted separately from misclassified pixels. In order to assess endmember fits on different endmember dates for each multi-temporal classification, RMSE results from MESMA were linked with each endmember date and class. Plots were created using ggplot2, an extension in R—a statistical computing software environment (www.r-project.org), and Microsoft Excel. Two species were singled out for in-depth date analysis, one tree species (*Quercus douglasii*; QUDO), and one shrub species (*Adenostoma fasciculatum*; ADFA). QUDO occurs in both savannah and woodland habitats, is drought-tolerant, and active into dry summers (Kueppers, Snyder, Sloan, Zavaleta, & Fulfrost, 2005). ADFA creates an overlapping branching canopy growing from March to June (Minnich, 1983). In late spring to early summer it develops white flowers, which turn brown and are retained through the summer. ADFA is also prone to drying in summer and fall (Lippitt, Stow, O'Leary, & Franklin, 2013). QUDO should have a more stable spectral profile in summer and fall, whereas ADFA should have more phenological variability in reflectance.

3. Results

3.1. Endmember libraries

IES run with a threshold of 0.01 RMSE produced endmember library sizes between 10 and 14% of the input training library size (Table 3). IES Kappa values for each endmember library ranged from 0.826 to 0.875, and demonstrated that the endmembers selected by IES were representative of the training libraries (Table 3). BAPI, PISA, QUAG, and EUSP had the highest proportion of their classes' training spectra selected for inclusion in the multi-temporal endmember library. ARCA-SALE, ERFA, and MAGF had the smallest proportion of their classes' training spectra selected. The total number of endmembers from each date selected by IES for the multi-temporal library varied between classes (Fig. 2). MAGF and BRNI had more endmembers selected for the multi-temporal library from earlier in the season, and relatively few from later in the season. CEME had nearly the same number of endmembers from each date. PLRA and ADFA had a higher proportion of endmembers selected from 30 Mar, 17 Jun and 26 Aug (Fig. 2).

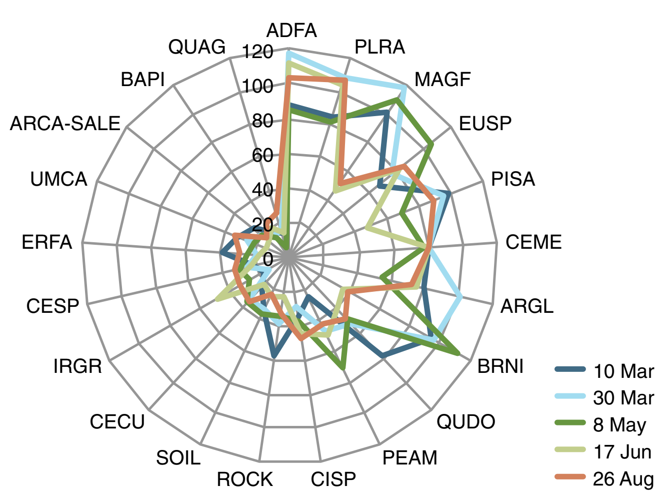

Fig. 2. Number of endmembers selected for each class, by endmember date, in the multi-temporal endmember library. Species abbreviations are listed in Table 2.

The total number of endmembers selected by IES from the multi-temporal training library (5379) was less than the number of endmembers that would result from combining the single-date endmember libraries (6211). For most species the number of endmembers selected from each date in the multi-temporal training library was lower than the mean number of endmembers selected for the single-date training libraries, indicating some redundancy of endmembers across dates. MAGF, ADFA, BRNI, and PLRA had a higher number of endmembers selected for the multi-temporal endmember library. These four classes had an average of 12.0, 8.8, 4.4, and 1.8 additional endmembers, respectively, compared to the mean number of endmembers for each class in the single-date endmember libraries.

3.2. Species classification

The spatial distribution of classes between same-date classifications and multi-temporal classifications shared similar patterns overall, but with sometimes key differences (Fig. 3). MAGF, BRNI, and ARGL were modeled in the same regions between classifications, though in the multi-temporal classification for 10 Mar, MAGF had an expanded range. For 10 Mar (Fig. 3a) the multi-temporal classification modeled more MAFG in place of BRNI. MAGF is commonly found with BRNI, but BRNI grows more slowly than MAGF. Thus areas dominated by MAGF in early March may become dominated by BRNI later in the season. *Ceanothus* species along with ADFA, QUAG, and ARGL also covered the same regions between classifications, but with sometimes very different abundances. For example, in the 17 Jun image (Fig. 3d) the same-date classification modeled very few ADFA pixels, while the multi-temporal classification modeled noticeably more. Also the dominant *Ceanothus* species varied between classifications, such as in 26 Aug (Fig. 3e), where CESP incorrectly dominates in the same-date classification. In the multi-temporal classification, these same areas are correctly mapped as CEME.

Overall accuracy for MESMA classification using the multi-temporal endmember library was comparable to same-date endmember libraries (Table 4). Same-date endmember libraries were able to classify images with overall accuracy between 67.9 and 76.4%. The multi-temporal endmember library had accuracies between 66.6 and 75.5%. The difference in performance between same-date and multi-temporal classifications was less than 1.3% in all cases. For two dates, 30 Mar and 26 Aug, the multi-temporal classification outperformed the same-date endmember library by 0.05 and 0.84% respectively. The percent of unclassified pixels was lowest using the multi-temporal endmember library (3–4%) compared to same-date libraries (4–5%). Significance testing of Kappa results between same-date and multi-temporal classification showed significant differences ($p < 0.05$) where the multi-temporal library underperformed the same-date library (10 Mar, 8 May, and 26 Aug), but differences in overall classification accuracy remained small (Table 4).

Producer's accuracies for all classes varied between good classification success with mean accuracies above 80% (ARCA-SALE, BRNI, ERFA, MAGF, SOIL) and poor accuracy below 50% (BAPI, PISA, QUAG) (Table 5). Eight to ten classes showed improved multi-temporal Producer's accuracy compared to same-date classifications. CEME, SOIL, and ROCK had higher Producer's accuracy for all dates in the multi-temporal classification. Classes which had the lowest Producer's accuracy compared to same-date results were CECU, BAPI, QUAG, and UMCA, with mean changes in accuracy ranging between −4.4% and −5.2%. CECU saw accuracy improvements of up to 12.6% but also reductions as low as −18.3% in the multi-temporal classifications when

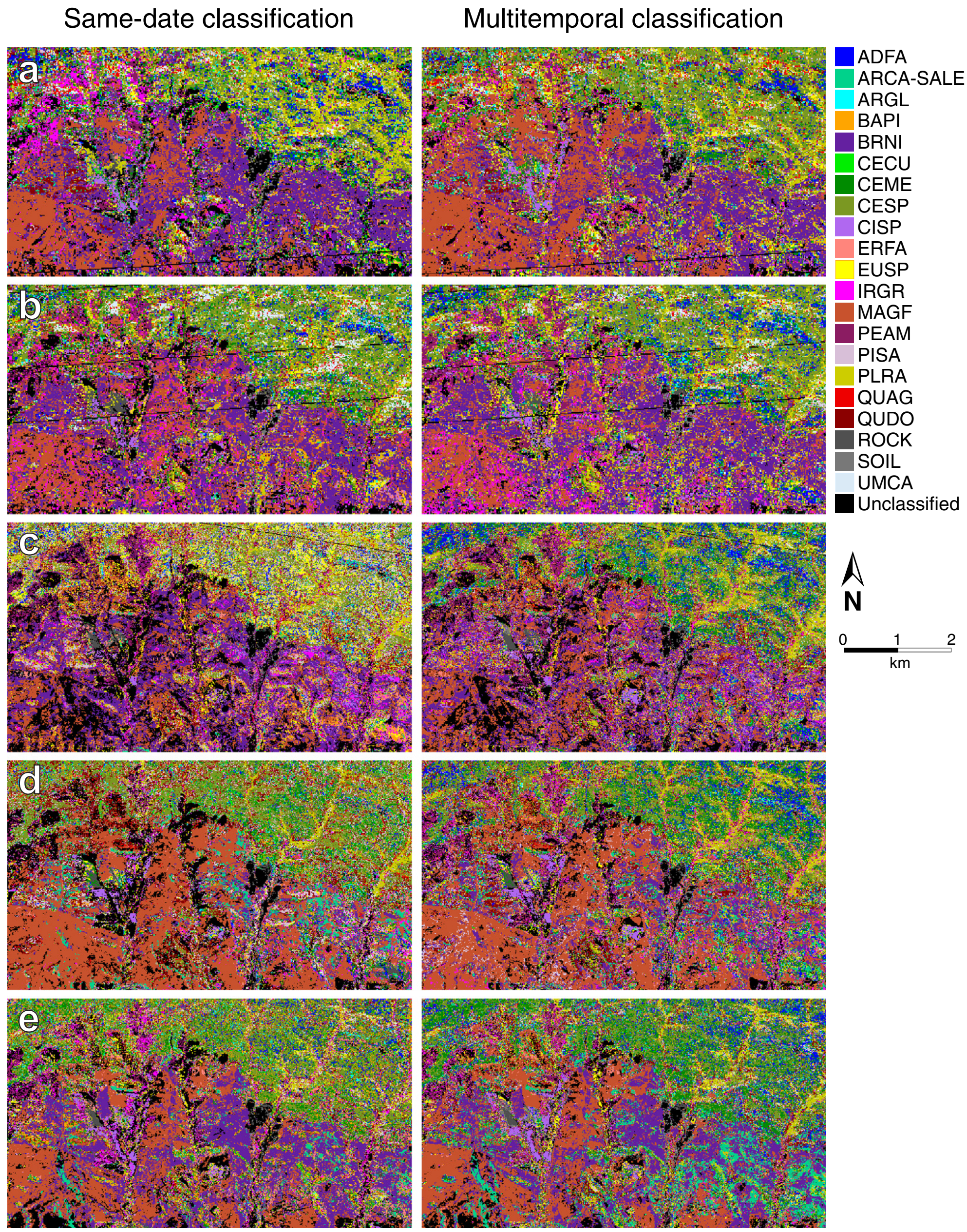

Fig. 3. Classification result of subregion (Fig. 1f1-sub) for same-date and multi-temporal classifications shown side by side. (a) 10 Mar; (b) 30 Mar; (c) 8 May; (d) 17 Jun; (e) 26 Aug. Lines across the May and two March images are caused by corrupted near infrared spectra for those pixels.

compared to same date classifications. Mean User's accuracy was higher for the multi-temporal classification for 10 out of 21 classes compared to same-date classifications (Table 6). User's accuracy was also frequently higher for individual classes when the multi-temporal library was applied on specific dates. Half of all classes had improvements in User's accuracy in the multi-temporal classification results.

Table 4
Overall accuracy (%) for all endmember libraries "EM date" (rows) used to classify image dates (columns). A RMSE threshold of 0.01 was used. The third row is the difference between the same-date (SD) endmember library and the multi-temporal (MT) endmember library. The final row is the z-score resulting from a kappa significance test comparing the same-date and multi-temporal classifications.

Library	Image date				
	10 Mar	30 Mar	8 May	17 Jun	26 Aug
SD	67.88	70.49	69.88	76.44	70.82
MT	66.58	70.54	68.82	75.46	71.66
Difference	−1.30	0.05	−1.06	−0.99	0.84
Z-score	2.23	0.01	2.65	2.71	1.78

3.3. Endmember temporal analysis

Spatial variation in the dates of endmembers selected from the multi-temporal endmember library used to map each pixel was apparent (Fig. 4). Endmembers selected to classify each pixel were most frequently from the same image date. Increased use of alternative endmember dates occurred where *Ceanothus* species were classified, which tended to choose endmembers with dates immediately preceding or following the date of the image. MAGF and BRNI, which senesce during seasonal drought, were heavily dominated by same-date endmembers. Agricultural zones tended to have more variable endmember dates.

Among correctly classified pixels, most classes used a majority of endmembers selected from the same date in the multi-temporal library

Table 5
Producer's accuracy (%) for same-date endmember libraries (Same) and the multi-temporal (MT) endmember library along with mean Producer's accuracy for each class. Shaded cells have a higher Producer's accuracy for the multi-temporal classification than same-date classification.

	10 Mar		30 Mar		8 May		17 Jun		26 Aug		Mean	
Class	Same	MT	Same	MT	Same	MT	Same	MT	Same	MT	Same	MT
ADFA	55.87	47.75	55.26	61.46	60.81	60.86	63.97	70.59	62.54	67.19	59.69	61.57
ARCA–SALE	83.81	85.64	83.65	83.30	88.37	85.82	96.45	92.47	91.15	92.11	88.69	87.87
ARGL	46.37	48.90	53.76	51.25	56.22	48.95	60.82	60.10	43.01	47.65	52.04	51.37
BAPI	35.81	29.73	41.35	29.32	38.70	37.33	54.15	52.16	40.34	27.80	42.07	35.27
BRNI	74.42	67.79	79.89	79.50	78.05	75.57	89.97	87.77	90.48	89.43	82.56	80.01
CECU	48.81	34.92	60.17	47.72	43.23	55.83	69.20	50.91	49.36	59.30	54.15	49.74
CEME	64.14	64.57	64.44	68.09	64.64	71.35	67.50	70.26	59.56	63.07	64.06	67.47
CESP	53.97	62.59	69.32	63.23	66.08	63.27	68.85	61.01	63.93	55.43	64.43	61.11
CISP	69.58	62.65	83.23	79.88	78.60	76.92	82.27	78.48	69.91	69.23	76.72	73.43
ERFA	84.11	78.41	82.51	87.80	90.04	88.68	91.28	93.50	90.17	89.95	87.62	87.67
EUSP	75.93	73.73	71.01	76.88	70.55	61.23	82.98	84.74	66.82	68.25	73.46	72.97
IRGR	76.69	72.30	72.95	75.00	61.37	63.74	78.65	78.50	70.66	59.13	72.06	69.73
MAGF	88.50	90.58	84.43	82.44	89.50	88.74	95.21	94.63	91.38	94.77	89.80	90.23
PEAM	70.75	74.09	71.10	73.12	62.13	64.34	65.95	66.19	64.43	60.76	66.87	67.70
PISA	27.72	27.29	46.58	44.52	33.37	27.26	33.87	23.58	41.21	38.09	36.55	32.15
PLRA	69.67	70.07	65.09	67.16	65.78	63.01	71.10	71.04	67.61	65.35	67.85	67.33
QUAG	56.25	39.58	40.88	21.17	49.33	22.82	41.54	38.46	47.25	39.16	47.05	32.24
QUDO	65.90	73.07	77.84	76.38	72.42	77.91	80.79	82.12	69.02	77.63	73.19	77.42
ROCK	47.46	48.02	56.69	63.06	62.00	67.14	67.54	70.18	57.18	61.58	58.17	62.00
SOIL	83.72	84.05	82.91	88.73	79.91	83.64	83.28	85.76	86.50	89.71	83.26	86.38
UMCA	68.72	54.19	65.35	63.37	58.25	58.87	70.24	62.55	64.29	61.84	65.37	60.16

(Fig. 5). Accuracy increased for some classes and declined for others when modeled with the multi-temporal library, compared to same-date classification accuracy. CEME, QUDO, and SOIL were classified by endmembers from a variety of dates, and also showed the most improvement in Producer's accuracy compared to same-date classifications. PLRA, BAPI, and EUSP showed little or no benefit from the multi-temporal library, with most endmembers coming from the same date (Fig. 5). For misclassified pixels half or more were typically drawn from same date endmembers, while the remaining half tended to be split between other endmember dates, with more

Table 6
User's accuracy (%) for same-date endmember libraries (Same) and the multi-temporal (MT) endmember library along with mean User's accuracy for each class. Shaded cells have a higher User's accuracy for the multi-temporal classification than same-date classification.

	10 Mar		30 Mar		8 May		17 Jun		26 Aug		Mean	
Class	Same	MT	Same	MT	Same	MT	Same	MT	Same	MT	Same	MT
ADFA	56.16	57.27	64.26	55.61	63.40	56.77	67.40	59.50	55.43	49.81	61.33	55.79
ARCA–SALE	80.45	77.73	87.52	85.94	88.57	88.27	96.66	95.94	95.85	91.98	89.81	87.97
ARGL	53.16	54.01	62.40	56.02	61.45	58.93	63.66	60.14	54.15	52.39	58.96	56.30
BAPI	60.92	43.14	47.83	54.93	45.93	47.60	60.82	62.80	42.50	78.10	51.60	57.31
BRNI	74.03	80.06	82.95	76.78	85.11	83.15	94.49	83.80	89.49	91.09	85.21	82.98
CECU	43.31	52.38	54.31	55.56	44.75	48.93	70.61	77.62	65.69	58.76	55.73	58.65
CEME	61.09	54.59	66.77	64.55	80.09	61.95	76.60	74.83	67.16	66.64	70.34	64.51
CESP	72.56	50.74	60.66	66.50	62.38	58.91	67.44	67.66	58.70	70.08	64.35	62.78
CISP	62.77	76.19	69.29	72.58	68.04	59.40	73.34	76.62	64.83	78.44	67.65	72.65
ERFA	83.11	87.64	84.51	85.16	83.84	88.01	91.75	91.34	86.35	87.20	85.91	87.87
EUSP	77.78	78.66	81.82	80.27	80.26	87.54	89.57	82.59	79.18	80.59	81.72	81.93
IRGR	74.92	81.68	78.31	68.22	68.04	74.09	72.06	69.49	64.75	68.70	71.62	72.44
MAGF	90.58	77.57	82.54	86.40	89.16	82.35	93.24	89.51	92.25	86.11	89.55	84.39
PEAM	75.82	72.48	71.51	74.63	68.42	70.38	71.95	66.51	65.34	62.99	70.61	69.40
PISA	47.45	46.04	52.99	60.37	43.59	62.31	51.95	61.12	50.90	61.32	49.38	58.23
PLRA	84.34	70.34	76.79	59.35	75.00	68.07	78.47	69.66	76.40	77.83	78.20	69.05
QUAG	50.63	39.86	57.73	44.62	52.50	51.91	52.12	61.58	60.33	62.69	54.66	52.13
QUDO	62.33	59.93	72.16	74.64	66.49	65.72	76.06	78.15	67.35	64.29	68.88	68.55
ROCK	70.59	84.16	65.44	86.84	73.31	77.81	80.21	79.47	74.14	69.77	72.74	79.61
SOIL	92.65	93.36	92.68	96.83	93.61	93.88	95.39	96.35	97.46	92.85	94.36	94.65
UMCA	62.90	59.71	63.16	63.05	58.99	56.97	64.38	73.75	66.32	70.14	63.15	64.72

Please cite this article as: Dudley, K.L., et al., A multi-temporal spectral library approach for mapping vegetation species across spatial and temporal phenological gradients, *Remote Sensing of Environment* (2015), http://dx.doi.org/10.1016/j.rse.2015.05.004

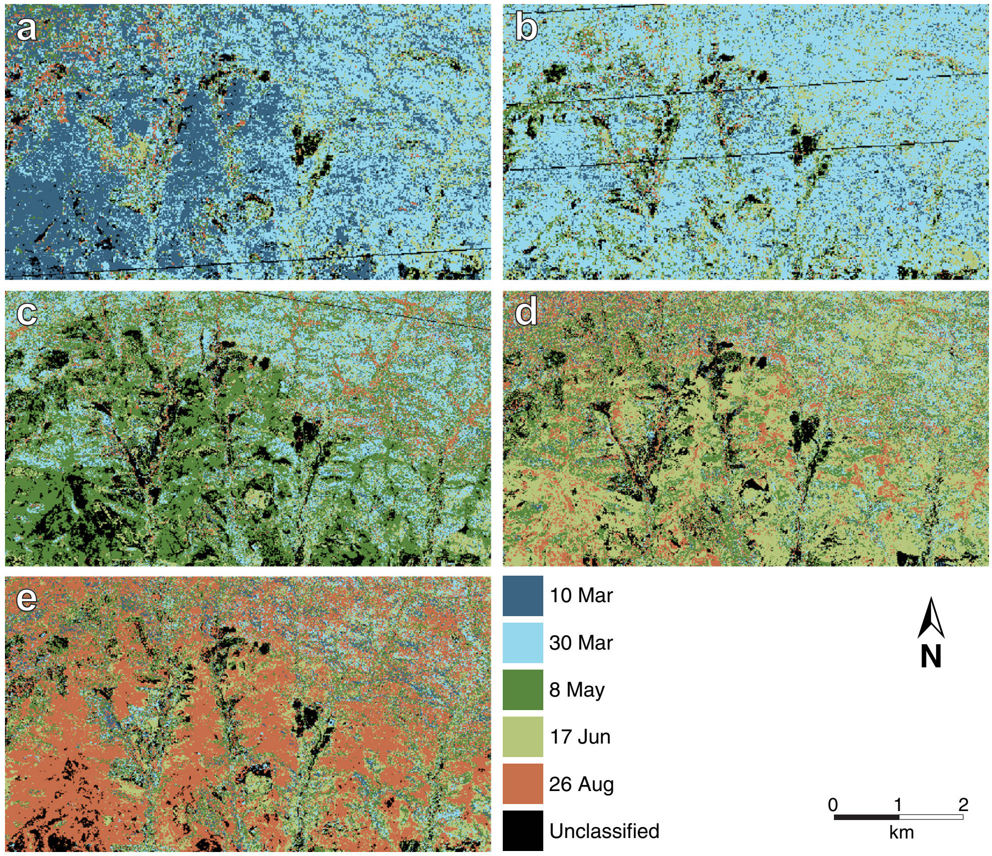

Fig. 4. Classification result of the f1 subset (Fig. 1) showing the date of endmembers from the multi-temporal endmember library used to classify pixels in images for (a) 10 Mar; (b) 30 Mar; (c) 8 May; (d) 17 Jun; and (e) 26 Aug.

misclassifications occurring for endmembers nearer to the date of the image (Fig. 5). While it appears that misclassified pixels were more commonly classified by a different date endmember than correctly classified pixels, classes such as CEME, ADFA, and QUDO still showed overall improvement using the multi-temporal library.

The correctly classified plots show the endmember date distribution of all correctly classified pixels for each image date (left column). The misclassified plots show the endmember date distribution of incorrectly classified pixels for each image date (right column). Note that y-axis scale changes between dates.

The distribution of endmember dates used for classification varied between image dates, with 17 Jun (Fig. 5) having the fewest endmembers from alternate dates. Comparatively few endmembers were used from alternate dates for the correctly classified pixels; of those endmembers selected from an alternate date, a majority tended to be from dates nearest to the image date. QUDO and ADFA were used as examples to determine how RMSE varied with the date of endmembers used for classification. Overall, QUDO selected more endmembers from differing dates than any other class, with more than half of the correctly classified pixels using alternate dates for the 17 Jun and 26 Aug classifications (Fig. 5). QUDO showed improvements in Producer's accuracy compared to the same-date classifications for 10 Mar (73.0%), 8 May (77.9%), 17 Jun (82.12%), and 26 Aug (77.6%), with lower accuracy for 30 Mar (76.4%) (Table 5). The majority of low RMSE values (associated with good model fits) for QUDO occurred when using same-date endmembers (Fig. 6). The remaining endmembers from alternate dates had higher overall RMSE values, with those nearer to the classified image date having lower RMSE values than those further away. ADFA, in contrast, tended towards using a higher proportion of same-date endmembers (Fig. 7). Like QUDO, endmembers from the same date as the image had lower RMSE. Fewer endmembers from other dates correctly modeled ADFA, likely due to greater temporal variability in ADFA spectra (Fig. 7).

4. Discussion

Larger endmember libraries are required by a multi-temporal approach (Table 3). While this increases the time required for MESMA to classify an image, it may be worth the increased processing time to improve flexibility in applying a single set of endmembers to imagery from any date with a minimal tradeoff in accuracy. The image dates in this study reflect the availability of data which covered the same sites within 2009. A broader range of dates may be more optimal, and needs to be tested to determine the effect that it might have on species classification accuracy. The ideal time of year for image acquisition may also vary greatly between species. Additionally, regions with subdued phenological cycles, such as some tropical forests, may benefit less from a multi-temporal library. Large regions with a greater range of phenologies present can show more variability in spectral response, which a multi-temporal library may be better able to model.

A multi-temporal endmember library approach worked well for images within the range of March to August. Dennison and Roberts (2003a) used endmembers selected by Endmember Average RMSE (EAR), a method for selecting endmembers based on minimum within-class RMSE, to classify species in AVIRIS images acquired over the Santa Barbara front range. They found that lower species classification accuracies occurred in water deficit images (Fall) compared to water surplus images (Spring). Endmember libraries created using IES for the 26 Aug 2009 image produced high overall accuracies for both the same-date library (70.8%) and the multi-temporal library (71.7%). Water deficit for an August image would be less extreme than the September images examined by Dennison and Roberts (2003a), but the

Please cite this article as: Dudley, K.L., et al., A multi-temporal spectral library approach for mapping vegetation species across spatial and temporal phenological gradients, *Remote Sensing of Environment* (2015), http://dx.doi.org/10.1016/j.rse.2015.05.004

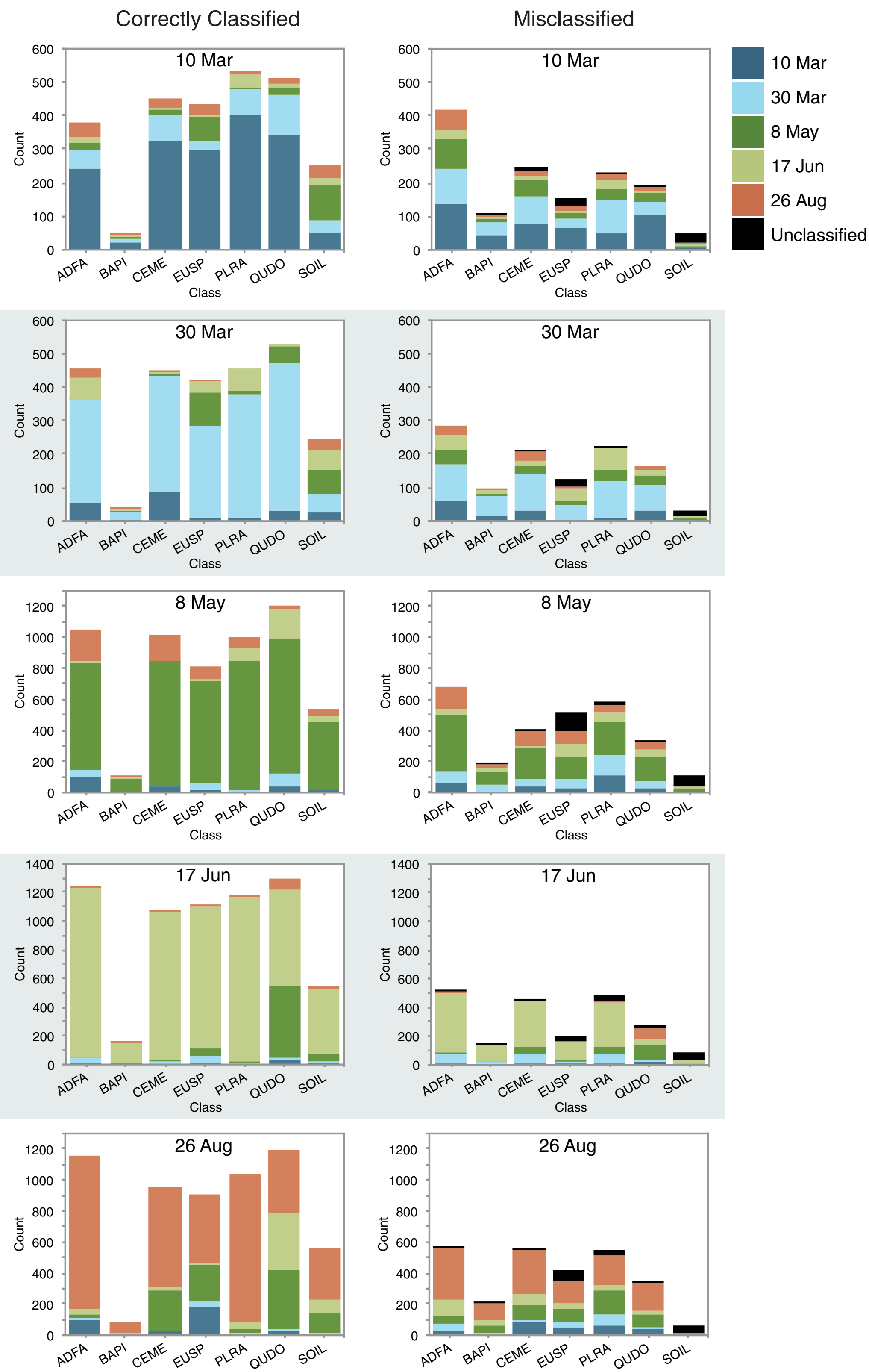

Fig. 5. Stacked bar plots of pixel counts for the multi-temporal endmember library classification results.

similar accuracies across all dates found in this study likely stem from differences between EAR and IES. EAR only accounts for how well an endmember classifies its own species, and does not account for whether selected endmembers increase misclassification of other species. In contrast, IES maximizes Kappa value, so endmembers that produce increased misclassification of other species are penalized. IES-selected endmember libraries were apparently able to overcome increased spectral variability caused by some seasonal drought stress without increasing misclassification as seen by Dennison and Roberts (2003a).

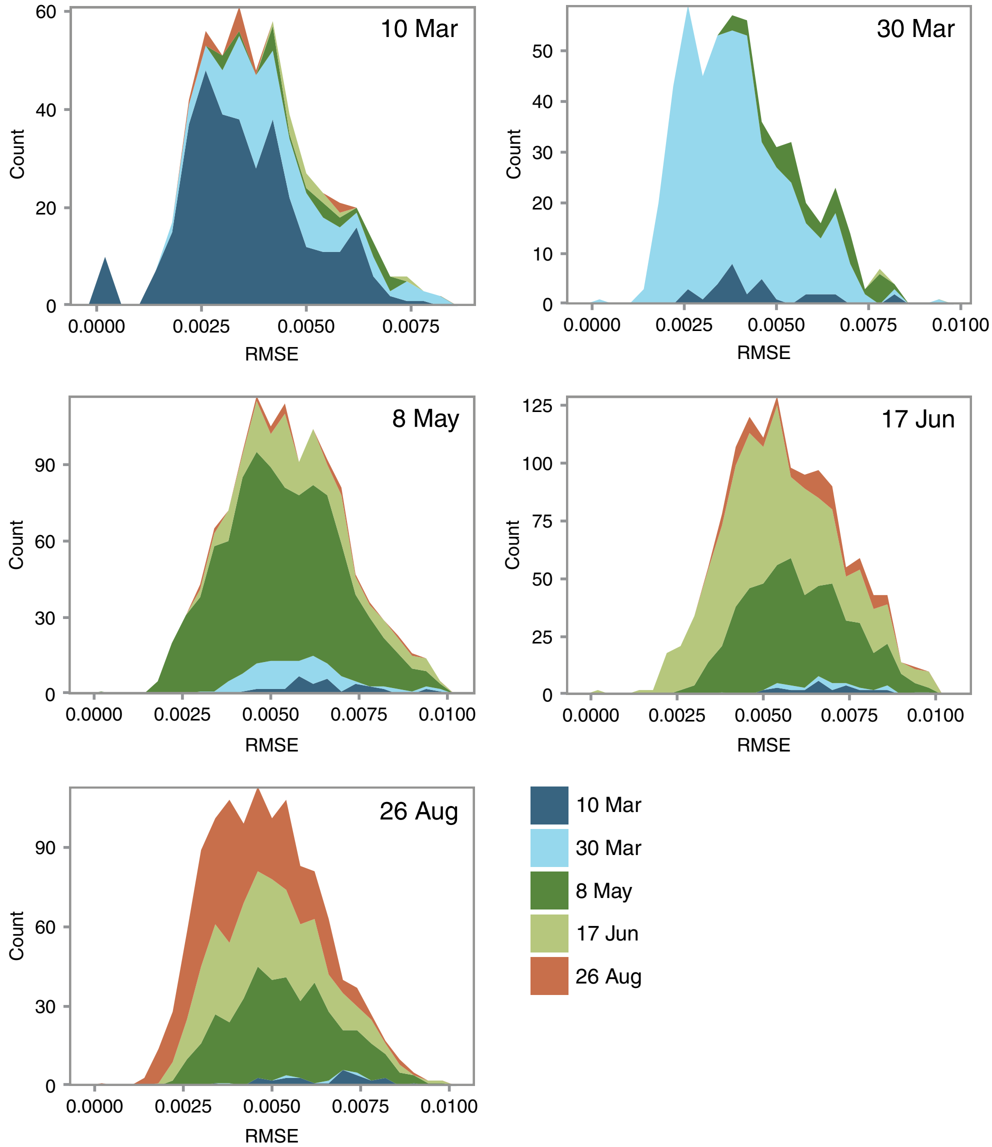

Fig. 6. Stacked histograms of pixel counts for endmember dates used from the multi-temporal endmember library for classifying QUDO, and the associated RMSE values from MESMA. These graphs show the distribution of correctly classified pixels. Note that the y-axis scale changes between graphs.

The multi-temporal endmember library produced overall accuracies that were within 1.3% of the accuracies for single-date libraries. At the species level there were important differences in how well the multi-temporal endmember library was leveraged, with some classes showing overall Producer's accuracy improvements (ADFA, CEME, ERFA, MAGF, PEAM, QUDO) between dates, others seeing greater penalties (BAPI, CECU, CESP, CISP, PISA, QUAG, UMCA), and still others with mixed results (ARCA-SALE, IRGR, PLRA). ROCK and SOIL classes had improved Producer's accuracy for all images using the multi-temporal library, indicating that classes which have few spectral differences within a season may benefit from an increase in reference spectra regardless of the season from which it was derived. Some species that demonstrate large changes in spectral reflectance due to phenology (e.g. MAGF and ADFA) benefited most from the use of a multi-temporal library.

Proportionally BAPI, PISA, and QUAG had the highest number of endmembers chosen for inclusion in all endmember libraries. These three classes also tended to have the lowest User's accuracy (39.9 to 78.1%) for single-date and multi-temporal classifications. ARCA-SALE, ERFA, and MAGF had the smallest proportion of endmembers selected from the available spectra in the training library. These classes also had the highest Producer's accuracies (78.4 to 96.5%) using the same-date and multi-temporal libraries, implying that seasonal spectral separability between these and other classes is high. For the multi-temporal library, the mean number of endmembers selected by IES for MAGF, ADFA, and BRNI was higher than all other classes. This may be a reflection of increased temporal variability in spectral response between dates.

The dominance of endmember dates used to classify a given species gives some hint to the level of spectral variability within each species over a season. For ADFA, correctly classified pixels in the 8 May, 17 Jun, and 26 Aug images were dominated by same-date endmembers (Fig. 7), demonstrating that ADFA had a more unique spectral signature later in the year, with fewer crossovers with other dates. This is supported by the mean spectra of ADFA endmembers from the multi-temporal library, with decreasing near infrared reflectance and increasing short-wave infrared reflectance for later dates (Fig. 8b). QUDO had more endmembers from different dates for 17 Jun and 26 Aug. This implies that QUDO was less spectrally variable than ADFA later in the season, as seen in the mean endmember spectra (Fig. 8).

Please cite this article as: Dudley, K.L., et al., A multi-temporal spectral library approach for mapping vegetation species across spatial and temporal phenological gradients, *Remote Sensing of Environment* (2015), http://dx.doi.org/10.1016/j.rse.2015.05.004

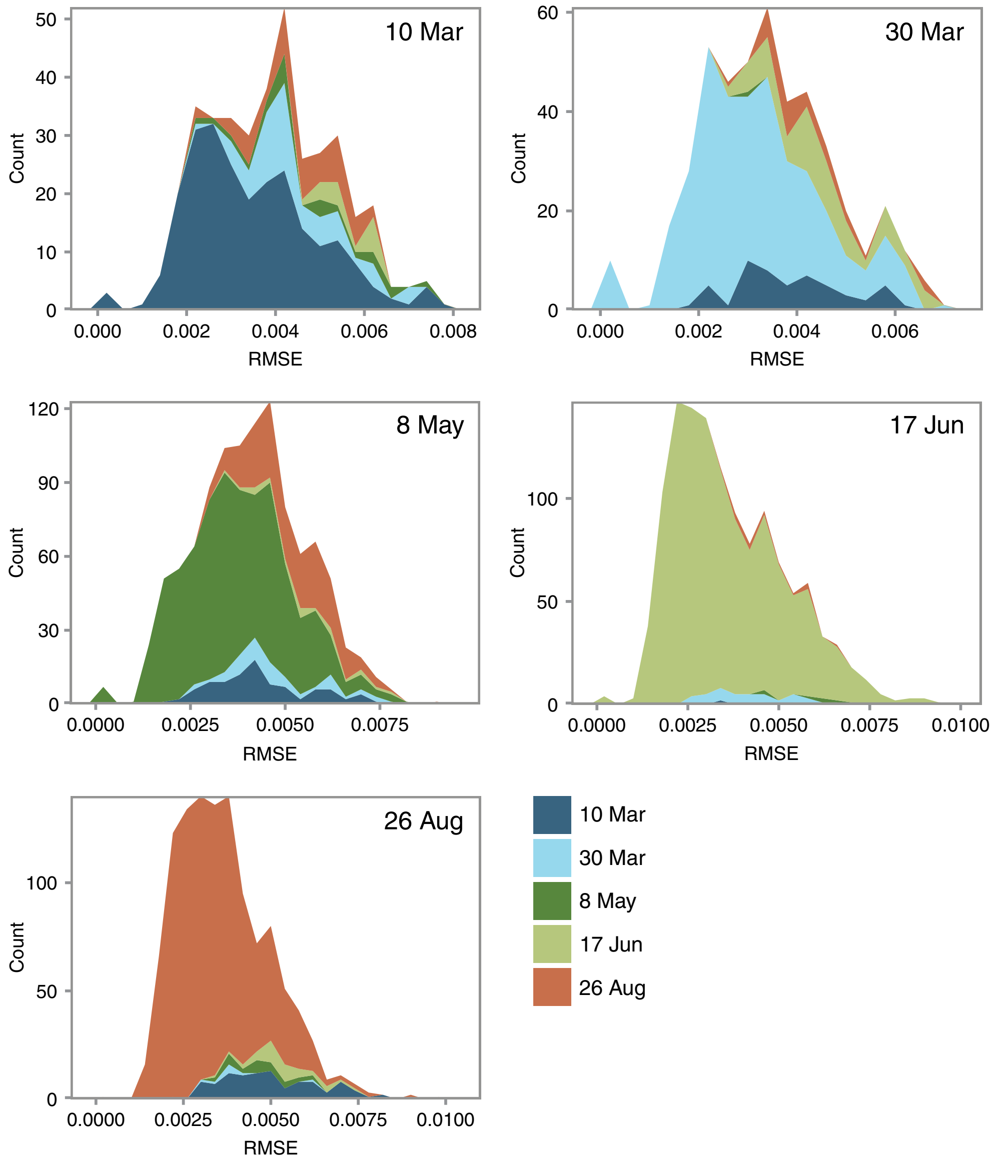

Fig. 7. Stacked histograms of pixel counts for endmember dates used from the multi-temporal library for ADFA and the associated RMSE values from MESMA. These graphs show the distribution of correctly classified pixels. Note that the y-axis scale changes between graphs.

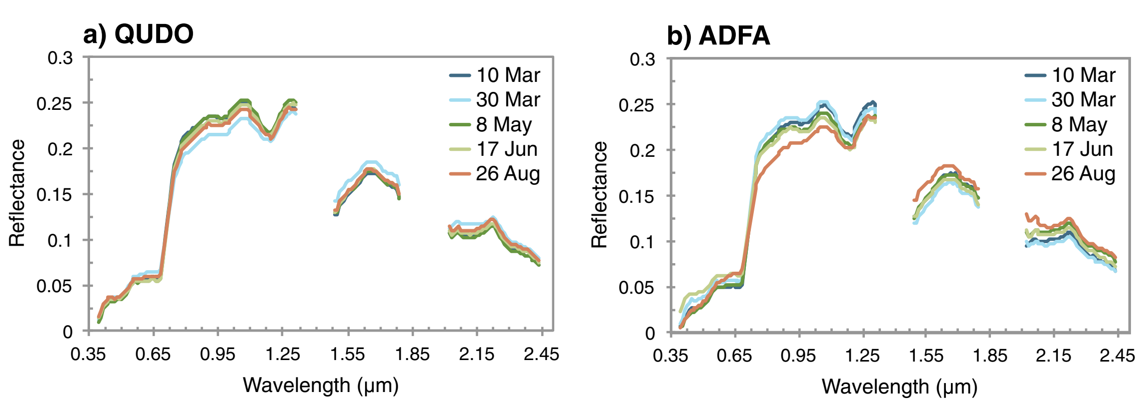

Fig. 8. Mean reflectance (by wavelength) for all multi-temporal library endmembers in QUDO (a) and ADFA (b) classes for each endmember date. Spectra have been normalized by mean reflectance across all wavelengths to correct for differences in overall brightness between dates.

Please cite this article as: Dudley, K.L., et al., A multi-temporal spectral library approach for mapping vegetation species across spatial and temporal phenological gradients, *Remote Sensing of Environment* (2015), http://dx.doi.org/10.1016/j.rse.2015.05.004

Other research has found that careful selection of spectra of the appropriate phenological phase is an important factor when classifying vegetation with varying spatial heterogeneity of phenology (Cole, McMorrow, & Evans, 2014; Dong et al., 2013; Peña-Barragán, López-Granados, Jurado-Expósito, & García-Torres, 2006). The proposed method may be useful when modeling large regions in which a phenological gradient occurs, such as a difference in green-up or senescence across a range of elevations. Endmembers appropriate for multiple phenophases could be included in the same endmember library. Using a multi-temporal endmember library along with the associated dates of the endmembers could be used to identify short- and long-term variability in phenology between species over large areas. Since a multi-temporal library's endmembers can be referenced by date, it is possible to identify which endmember dates are dominant in classifying an image. Those in turn can be used to indicate the dominant seasonal signal or climatic conditions of an image or its subregions. A combination of hyperspectral imagery and multi-temporal scenes could provide information on a large range of phenological variations between and within species through multiple seasons.

5. Conclusions

This paper examined the ability of a multi-temporal endmember library created with IES and classified with MESMA two-endmember models to determine if a phenologically inclusive endmember library could be used in place of single-date endmember libraries. IES can greatly reduce and simplify an input spectral library to decrease the computational load for processing two-endmember MESMA classifications without the need of excessive user interaction. IES was able to maintain high species-level classification accuracy using a single multi-temporal endmember library, despite the potential for spectral confusion when comparing spectra across multiple dates. This method could potentially increase accuracy and flexibility when applying spectral libraries to images where sufficient training datasets are unavailable for single-date classification. With spaceborne hyperspectral sensors on the horizon, repeat hyperspectral images will become more accessible in the future and building regional phenological spectral libraries can be more easily achieved.

The planned NASA HyspIRI mission, which will include a hyperspectral visible-shortwave infrared (VSWIR) sensor, represents new access to repeat acquisition high spectral resolution imagery. HyspIRI presents an opportunity to incorporate phenological effects into species mapping that have so far been unavailable. This study illustrates how HyspIRI-like data could potentially improve vegetation classification methods using phenology when classifying single-date imagery. Tracking changes in phenology have proven a useful tool for assessing climate change impacts in broad regions using MODIS imagery (Ivits et al., 2012; Panday & Ghimire, 2012). Biologists and ecologists could use multi-date endmember libraries to track phenological timing with a more species-specific focus than current methods, which tend to rely on coarse scale MODIS NDVI-based phenology.

Timing of phenological events may not be consistent between years, and phenology may become increasingly variable due to climate change (Badeck et al., 2004; Begue, Vintrou, Saad, & Hiernaux, 2014; Garonna et al., 2014; Girard, Beaudet, Mailly, & Messier, 2014; Guan, 2014; Park & Schwartz, 2014; Pilaš, Medved, Medak, & Medak, 2014; Schwartzberg et al., 2014). A single-date endmember library used between years may be a poor match to subsequent years if climate or other factors differ between library creation and application. A multi-temporal endmember library could be more easily applied to images year to year, as it can include a broader range of phenological conditions than single-date libraries. However, a multi-temporal endmember library is much larger than a single-date library and end-users will need to determine if their species of focus will benefit from multi-temporal datasets. Analyses of large scale landscapes could potentially include several phenologies between and within species. Phenologically inclusive endmember libraries and endmember date analysis provide a means to understand diverse regions and species through time.

Acknowledgments

We would like to thank Michael Toomey, Seth Peterson, and Michael Alonzo for their assistance in collecting field data and processing the image data. Funding for this study was provided by NASA grant #NNX12AP08G.

References

Adams, J. B., Smith, M. O., & Gillespie, A. R. (1993). Imaging spectroscopy: interpretation based on spectral mixture analysis. In C. M. Pieters, & P. A. Englert (Eds.), *Remote Geochemical Analysis, Elemental and Mineralogical Composition* (pp. 145–166) (1st ed.). Cambridge, England: Press Syndicate of Univ. of Cambridge.

Asner, G. P., Jones, M. O., Martin, R. E., Knapp, D. E., & Hughes, R. F. (2008). Remote sensing of native and invasive species in Hawaiian forests. *Remote Sensing of Environment*, *112*(5), 1912–1926. http://dx.doi.org/10.1016/j.rse.2007.02.043.

Badeck, F. W., Bondeau, A., Böttcher, K., Doktor, D., Lucht, W., Schaber, J., et al. (2004). Responses of spring phenology to climate change. *New Phytologist*, *162*(2), 295–309. http://dx.doi.org/10.1111/j.1469-8137.2004.01059.x.

Begue, A., Vintrou, E., Saad, A., & Hiernaux, P. (2014). Differences between cropland and rangeland MODIS phenology (start-of-season) in Mali. *ITC Journal*. http://dx.doi.org/10.1016/j.jag.2014.03.024.

Borel, C. C., & Gerstl, S. A. W. (1994). Nonlinear spectral mixing models for vegetative and soil surfaces. *Remote Sensing of Environment*, *47*(3), 403–416. http://dx.doi.org/10.1016/0034-4257(94)90107-4.

Clark, M. L., Roberts, D. A., & Clark, D. B. (2005). Hyperspectral discrimination of tropical rain forest tree species at leaf to crown scales. *Remote Sensing of Environment*, *96*(3–4), 375–398. http://dx.doi.org/10.1016/j.rse.2005.03.009.

Cochrane, M. A. (2000). Using vegetation reflectance variability for species level classification of hyperspectral data. *International Journal of Remote Sensing*, *21*(10), 2075–2087.

Cohen, J. (1960). A coefficient of agreement for nominal scales. *Educational and Psychological Measurement*, *20*(1), 37–46. http://dx.doi.org/10.1177/001316446002000104.

Cole, B., McMorrow, J., & Evans, M. (2014). Spectral monitoring of moorland plant phenology to identify a temporal window for hyperspectral remote sensing of peatland. *ISPRS Journal of Photogrammetry and Remote Sensing*, *90*, 49–58. http://dx.doi.org/10.1016/j.isprsjprs.2014.01.010.

Congalton, R. G. (1991). A review of assessing the accuracy of classifications of remotely sensed data. *Remote Sensing of Environment*, *37*(1), 35–46. http://dx.doi.org/10.1016/0034-4257(91)90048-B.

Dehaan, R., Louis, J., Wilson, A., Hall, A., & Rumbachs, R. (2007). Discrimination of blackberry (*Rubus fruticosus* sp. agg.) using hyperspectral imagery in Kosciuszko National Park, NSW, Australia. *ISPRS Journal of Photogrammetry and Remote Sensing*, *62*(1), 13–24. http://dx.doi.org/10.1016/j.isprsjprs.2007.01.004.

Delalieux, S., Somers, B., Haest, B., Spanhove, T., Vanden Borre, J., & Mücher, C. A. (2012). Heathland conservation status mapping through integration of hyperspectral mixture analysis and decision tree classifiers. *Remote Sensing of Environment*, *126*, 222–231. http://dx.doi.org/10.1016/j.rse.2012.08.029.

Dennison, P. E., Charoensiri, K., Roberts, D. A., Peterson, S. H., & Green, R. O. (2006). Wildfire temperature and land cover modeling using hyperspectral data. *Remote Sensing of Environment*, *100*(2), 212–222. http://dx.doi.org/10.1016/j.rse.2005.10.007.

Dennison, P. E., & Roberts, D. A. (2003a). The effects of vegetation phenology on endmember selection and species mapping in southern California chaparral. *Remote Sensing of Environment*, *87*(2–3), 295–309. http://dx.doi.org/10.1016/j.rse.2003.07.001.

Dennison, P. E., & Roberts, D. A. (2003b). Endmember selection for multiple endmember spectral mixture analysis using endmember average RMSE. *Remote Sensing of Environment*, *87*(2–3), 123–135. http://dx.doi.org/10.1016/S0034-4257(03)00135-4.

Dong, J., Xiao, X., Chen, B., Torbick, N., Jin, C., Zhang, G., et al. (2013). Mapping deciduous rubber plantations through integration of PALSAR and multi-temporal Landsat imagery. *Remote Sensing of Environment*, *134*, 392–402. http://dx.doi.org/10.1016/j.rse.2013.03.014.

Franke, J., Roberts, D. A., Halligan, K., & Menz, G. (2009). Hierarchical Multiple Endmember Spectral Mixture Analysis (MESMA) of hyperspectral imagery for urban environments. *Remote Sensing of Environment*, *113*(8), 1712–1723. http://dx.doi.org/10.1016/j.rse.2009.03.018.

Franklin, J., Regan, H. M., & Syphard, A. D. (2014). Linking spatially explicit species distribution and population models to plan for the persistence of plant species under global change. *Environmental Conservation*, *41*(2), 97–109. http://dx.doi.org/10.1017/S0376892913000453.

Garonna, I., de Jong, R., de Wit, A. J., Mücher, C. A., Schmid, B., & Schaepman, M. E. (2014). Strong contribution of autumn phenology to changes in satellite-derived growing season length estimates across Europe (1982–2011). *Global Change Biology*. http://dx.doi.org/10.1111/gcb.12625.

Girard, F., Beaudet, M., Mailly, D., & Messier, C. (2014). Integrating climatic response in competition dependent tree-level growth models for northern hardwoods. *Forest Ecology and Management*, *323*, 138–147. http://dx.doi.org/10.1016/j.foreco.2014.03.014.

Guan, B. T. (2014). Ensemble empirical mode decomposition for analyzing phenological responses to warming. *Agricultural and Forest Meteorology*, *194*, 1–7. http://dx.doi.org/10.1016/j.agrformet.2014.03.010.

Hamada, Y., Stow, D. A., Roberts, D. A., Franklin, J., & Kyriakidis, P. C. (2012). Assessing and monitoring semi-arid shrublands using object-based image analysis and multiple endmember spectral mixture analysis. *Environmental Monitoring and Assessment*, 1–18. http://dx.doi.org/10.1007/s10661-012-2781-z.

Hestir, E. L., Khanna, S., Andrew, M. E., Santos, M. J., Viers, J. H., Greenberg, J. A., et al. (2008). Identification of invasive vegetation using hyperspectral remote sensing in the California Delta ecosystem. *Remote Sensing of Environment*, *112*(11), 4034–4047. http://dx.doi.org/10.1016/j.rse.2008.01.022.

Ishii, J., Lu, S., Funakoshi, S., Shimizu, Y., Omasa, K., & Washitani, I. (2009). Mapping potential habitats of threatened plant species in a moist tall grassland using hyperspectral imagery. *Biodiversity and Conservation*, *18*(9), 2521–2535. http://dx.doi.org/10.1111/j.1469-8137.1979.tb02312.x.

Ivits, E., Cherlet, M., Tóth, G., Sommer, S., Mehl, W., Vogt, J., et al. (2012). Combining satellite derived phenology with climate data for climate change impact assessment. *Global and Planetary Change*, *88–89*, 85–97. http://dx.doi.org/10.1016/j.gloplacha.2012.03.010.

Janssen, L. L. F., & van der Wel, F. J. M. (1994). Accuracy assessment of satellite derived land-cover data: a review. *Photogrammetric Engineering and Remote Sensing*, *60*(4), 419–426.

Keshava, N., & Mustard, J. F. (2002). Spectral unmixing. *IEEE Signal Processing Magazine*, *19*(1), 44–57. http://dx.doi.org/10.1109/79.974727.

Kueppers, L. M., Snyder, M. A., Sloan, L. C., Zavaleta, E. S., & Fulfrost, B. (2005). Modelled regional climate change and California endemic oak ranges. *Proceedings of the National Academy of Sciences of the United States of America*, *102*(45), 16281–16286. http://dx.doi.org/10.1073/pnas.0501427102.

Li, L., Ustin, S. L., & Lay, M. (2005). Application of multiple endmember spectral mixture analysis (MESMA) to AVIRIS imagery for coastal salt marsh mapping: a case study in China Camp, CA, USA. *International Journal of Remote Sensing*, *26*(23), 5193–5207. http://dx.doi.org/10.1080/01431160500218911.

Liao, C. H., Zhang, X. F., & Liu, Y. (2012). Remote sensing retrieval of vegetation coverage in arid areas based on multiple endmember spectral unmixing. *Chinese Journal of Applied Ecology*, *23*(12), 3243–3249.

Lieth, H. (1974). *Phenology and Seasonality Modeling* (1st ed.). London: Chapman and Hall.

Lippitt, C. L., Stow, D. A., O'Leary, J. F., & Franklin, J. (2013). Influence of short-interval fire occurrence on post-fire recovery of fire-prone shrublands in California, USA. *International Journal of Wildland Fire*, *22*(2), 184–193. http://dx.doi.org/10.1071/WF10099.

López-Granados, F., Jurado-Expósito, M., Peña-Barragan, J. M., & García-Torres, L. (2006). Using remote sensing for identification of late-season grass weed patches in wheat. *Weed Science*, *54*(2), 346–353. http://dx.doi.org/10.1043/0043-1745(2006)54[346:URSFIO]2.0.CO;2.

Mannel, S., & Price, M. (2012). Comparing classification results of multi-seasonal TM against AVIRIS imagery — seasonality more important than number of bands. *Photogrammetrie, Fernerkundung, Geoinformation*, *2012*(5), 603–612. http://dx.doi.org/10.1127/1432-8364/2012/0142.

Meentemeyer, R. K., & Moody, A. (2000). Rapid sampling of plant species composition for assessing vegetation patterns in rugged terrain. *Landscape Ecology*, *15*(8), 697–711. http://dx.doi.org/10.1023/A:1008175612254.

Michishita, R., Gong, P., & Xu, B. (2012). Spectral mixture analysis for bi-sensor wetland mapping using Landsat TM and Terra MODIS data. *International Journal of Remote Sensing*, *33*(11), 3373–3401. http://dx.doi.org/10.1080/01431161.2011.611185.

Minnich, R. A. (1983). Fire mosaics in southern California and northern Baja California. *Science*, *219*(4590), 1287–1294. http://dx.doi.org/10.1126/science.219.4590.1287.

Nidamanuri, R. R., & Zbell, B. (2011). Use of field reflectance data for crop mapping using airborne hyperspectral image. *ISPRS Journal of Photogrammetry and Remote Sensing*, *66*(5), 683–691. http://dx.doi.org/10.1016/j.isprsjprs.2011.05.001.

Okin, G. S., Clarke, K. D., & Lewis, M. M. (2013). Comparison of methods for estimation of absolute vegetation and soil fractional cover using MODIS normalized BRDF-adjusted reflectance data. *Remote Sensing of Environment*, *130*, 266–279. http://dx.doi.org/10.1016/j.rse.2012.11.021.

Panday, P. K., & Ghimire, B. (2012). Time-series analysis of NDVI from AVHRR data over the Hindu Kush–Himalayan region for the period 1982–2006. *International Journal of Remote Sensing*, *33*(21), 6710–6721. http://dx.doi.org/10.1080/01431161.2012.692836.

Papeş, M., Tupayachi, R., Martínez, P., Peterson, A. T., & Powell, G. V. N. (2010). Using hyperspectral satellite imagery for regional inventories: a test with tropical emergent trees in the Amazon Basin. *Journal of Vegetation Science*, *21*(2), 342–354. http://dx.doi.org/10.1111/j.1654-1103.2009.01147.x.

Park, I. W., & Schwartz, M. D. (2014). Long-term herbarium records reveal temperature-dependent changes in flowering phenology in the southeastern USA. *International Journal of Biometeorology*. http://dx.doi.org/10.1007/s00484-014-0846-0.

Peña-Barragán, J. M., López-Granados, F., Jurado-Expósito, M., & García-Torres, L. (2006). Spectral discrimination of *Ridolfia segetum* and sunflower as affected by phenological stage. *Weed Research*, *46*(1), 10–21. http://dx.doi.org/10.1111/j.1365-3180.2006.00488.x.

Pilaš, I., Medved, I., Medak, J., & Medak, D. (2014). Response strategies of the main forest types to climatic anomalies across Croatian biogeographic regions inferred from FAPAR remote sensing data. *Forest Ecology and Management*, *326*, 58–78. http://dx.doi.org/10.1016/j.foreco.2014.04.012.

Potgieter, A. B., Apan, A., Dunn, P., & Hammer, G. (2007). Estimating crop area using seasonal time series of enhanced vegetation index from MODIS satellite imagery. *Australian Journal of Agricultural Research*, *58*(4), 316–325. http://dx.doi.org/10.1071/AR06279.

Powell, R. L., Roberts, D. A., Dennison, P. E., & Hess, L. L. (2007). Sub-pixel mapping of urban land cover using multiple endmember spectral mixture analysis: Manaus, Brazil. *Remote Sensing of Environment*, *106*(2), 253–267. http://dx.doi.org/10.1016/j.rse.2006.09.005.

Ray, T. W., & Murray, B. C. (1996). Nonlinear spectral mixing in desert vegetation. *Remote Sensing of Environment*, *55*(1), 59–64.

Richter, R., & Schläpfer, D. (2002). Geo-atmospheric processing of airborne imaging spectrometry data. Part 2: atmospheric/topographic correction. *International Journal of Remote Sensing*, *23*(13), 2631–2649. http://dx.doi.org/10.1080/01431160110115834.

Riordan, E. C., & Rundel, P. W. (2014). Land use compounds habitat losses under projected climate change in a threatened California ecosystem. *PLoS ONE*, *9*(1). http://dx.doi.org/10.1371/journal.pone.0086487.

Roberts, D. A., Dennison, P. E., Roth, K. L., Dudley, K., & Hulley, G. (2015). Relationships between dominant plant species, fractional cover and Land Surface Temperature in a Mediterranean ecosystem. *Remote Sensing of Environment*. http://dx.doi.org/10.1016/j.rse.2015.01.026.

Roberts, D. A., Gardner, M., Church, R., Ustin, S., Scheer, G., & Green, R. O. (1998). Mapping chaparral in the Santa Monica Mountains using multiple endmember spectral mixture models. *Remote Sensing of Environment*, *65*(3), 267–279. http://dx.doi.org/10.1016/S0034-4257(98)00037-6.

Roberts, D. A., Quattrochi, D. A., Hulley, G. C., Hook, S. J., & Green, R. O. (2012). Synergies between VSWIR and TIR data for the urban environment: an evaluation of the potential for the Hyperspectral Infrared Imager (HyspIRI) Decadal Survey mission. *Remote Sensing of Environment*, *117*, 83–101. http://dx.doi.org/10.1016/j.rse.2011.07.021.

Roberts, D. A., Smith, M. O., & Adams, J. B. (1993). Green vegetation, nonphotosynthetic vegetation, and soils in AVIRIS data. *Remote Sensing of Environment*, *44*(2–3), 255–269. http://dx.doi.org/10.1016/0034-4257(93)90020-X.

Rosso, P. H., Ustin, S. L., & Hastings, A. (2005). Mapping marshland vegetation of San Francisco Bay, California, using hyperspectral data. *International Journal of Remote Sensing*, *26*(23), 5169–5191. http://dx.doi.org/10.1080/01431160500218770.

Roth, K. L., Dennison, P. E., & Roberts, D. A. (2012). Comparing endmember selection techniques for accurate mapping of plant species and land cover using imaging spectrometer data. *Remote Sensing of Environment*, *127*, 139–152. http://dx.doi.org/10.1016/j.rse.2012.08.030.

Schaaf, A., Dennison, P., Fryer, G., Roth, K., & Roberts, D. (2011). Mapping plant functional types at multiple spatial resolutions using imaging spectrometer data. *GIScience and Remote Sensing*, *48*(3), 324–344. http://dx.doi.org/10.2747/1548-1603.48.3.324.

Schmidt, K. S., & Skidmore, A. K. (2003). Spectral discrimination of vegetation types in a coastal wetland. *Remote Sensing of Environment*, *85*(1), 92–108. http://dx.doi.org/10.1016/S0034-4257(02)00196-7.

Schwartzberg, E. G., Jamieson, M. A., Raffa, K. F., Reich, P. B., Montgomery, R. A., & Lindroth, R. L. (2014). Simulated climate warming alters phenological synchrony between an outbreak insect herbivore and host trees. *Oecologia*. http://dx.doi.org/10.1007/s00442-014-2960-4.

Somers, B., & Asner, G. P. (2012). Invasive species mapping in Hawaiian rainforests using multi-temporal hyperion spaceborne imaging spectroscopy. *IEEE Journal of Selected Topics in Applied Earth Observations and Remote Sensing*. http://dx.doi.org/10.1109/JSTARS.2012.2203796.

Somers, B., & Asner, G. P. (2013). Multi-temporal hyperspectral mixture analysis and feature selection for invasive species mapping in rainforests. *Remote Sensing of Environment*, *136*, 14–27. http://dx.doi.org/10.1016/j.rse.2013.04.006.

Somers, B., Zortea, M., Plaza, A., & Asner, G. P. (2012). Automated extraction of image-based endmember bundles for improved spectral unmixing. *IEEE Journal of Selected Topics in Applied Earth Observations and Remote Sensing*, *5*(2), 396–408. http://dx.doi.org/10.1109/JSTARS.2011.2181340.

Sonnentag, O., Chen, J. M., Roberts, D. A., Talbot, J., Halligan, K. Q., & Govind, A. (2007). Mapping tree and shrub leaf area indices in an ombrotrophic peatland through multiple endmember spectral unmixing. *Remote Sensing of Environment*, *109*(3), 342–360. http://dx.doi.org/10.1016/j.rse.2007.01.010.

Thorp, K. R., French, A. N., & Rango, A. (2013). Effect of image spatial and spectral characteristics on mapping semi-arid rangeland vegetation using multiple endmember spectral mixture analysis (MESMA). *Remote Sensing of Environment*, *132*, 120–130. http://dx.doi.org/10.1016/j.rse.2013.01.008.

Tompkins, S., Mustard, J. F., Pieters, C. M., & Forsyth, D. W. (1997). Optimization of endmembers for spectral mixture analysis. *Remote Sensing of Environment*, *59*(3), 472–489. http://dx.doi.org/10.1016/S0034-4257(96)00122-8.

Ullah, S., Schlerf, M., Skidmore, A. K., & Hecker, C. (2012). Identifying plant species using mid-wave infrared (2.5–6 μm) and thermal infrared (8–14 μm) emissivity spectra. *Remote Sensing of Environment*, *118*(0), 95–102. http://dx.doi.org/10.1016/j.rse.2011.11.008.

Walker, J. J., de Beurs, K. M., & Wynne, R. H. (2014). Dryland vegetation phenology across an elevation gradient in Arizona, USA, investigated with fused MODIS and landsat data. *Remote Sensing of Environment*, *144*, 85–97. http://dx.doi.org/10.1016/j.rse.2014.01.007.

Wardlow, B. D., & Egbert, S. L. (2010). A comparison of MODIS 250-m EVI and NDVI data for crop mapping: a case study for southwest Kansas. *International Journal of Remote Sensing*, *31*(3), 805–830. http://dx.doi.org/10.1080/01431160902897858.

Yamano, H., Chen, J., & Tamura, M. (2003). Hyperspectral identification of grassland vegetation in Xilinhot, Inner Mongolia, China. *International Journal of Remote Sensing*, *24*(15), 3171–3178.

Youngentob, K. N., Roberts, D. A., Held, A. A., Dennison, P. E., Jia, X., & Lindenmayer, D. B. (2011). Mapping two *Eucalyptus subgenera* using multiple endmember spectral mixture analysis and continuum-removed imaging spectrometry data. *Remote Sensing of Environment*, *115*(5), 1115–1128. http://dx.doi.org/10.1016/j.rse.2010.12.012.

Zhang, J., Zhang, J., & Xu, Y. (2012). *Detecting Major Phenological Stages of Rice Using MODIS-EVI Data and Symlet11 Wavelet in Northeast China, Nanjing.*

Zhong, L., Gong, P., & Biging, G. S. (2012). Phenology-based crop classification algorithm and its implications on agricultural water use assessments in California's Central Valley. *Photogrammetric Engineering and Remote Sensing*, *78*(8), 799–813.

Zomer, R. J., Trabucco, A., & Ustin, S. L. (2009). Building spectral libraries for wetlands land cover classification and hyperspectral remote sensing. *Journal of Environmental Management*, *90*(7), 2170–2177. http://dx.doi.org/10.1016/j.jenvman.2007.06.028.